Quantifying Carrier Selective Contacts

in Solar Cells

by

Priyaranga L Koswatta

A Thesis Presented in Partial Fulfillment
of the Requirements for the Degree
Master of Science

Approved February 2016 by the
Graduate Supervisory Committee:

Zachary Holman, Chair
Richard King
Mariana Bertoni

ARIZONA STATE UNIVERSITY

May 2016

ABSTRACT

A basic theory and terminology that comprehensively applies to all different types of contacts in silicon solar cells has, thus far, been elusive. While the well established diode model has been applied to many of the complex contacts, the theory is not adequate to intuitively describe the characteristics of novel contacts. This thesis shows that the many desirable characteristics of contacts that are discussed in the literature—carrier selectivity, passivation, and low majority carrier conductance, key among them—originate from the resistance to electrons and holes in the contact. These principles are applied to describe a few popular contact technologies in order to pave the path to envisioning novel contacts. Metrics for contact performance is introduced to quantify each of the above characteristics using the two carrier resistances. The the validity of the proposed metrics is explored using extensive PC-1D simulations.

To my wife and family.

ACKNOWLEDGMENTS

I would like to thank my research adviser, Dr. Zachary Holman. His dedication, patience, and commitment helped me strive to be a better researcher and persevere to achieve a higher standard. His meticulous eye for detail and pursuit for perfection has encouraged me to do the same in my work.

I would also like to thank Dr. Mathieu Boccard for being a guide and a friend. The weekly discussions that we had with Dr. Holman was the key to the success of this project.

I would also like to thank my committee, Dr. Mariana Bertoni and Dr. Richard King, for taking time out from their busy schedule to guide me to improve this work. Their knowledge in their respective fields is highly respected and I am honored to have them in my committee.

I would also like to thank my friends and colleagues at ASU, Brad, Tim, Joe, April, Sebastian, Prateek, Salman, Jason, Mark, Mehdi, Sri, and Laura for their insightful discussions and continual encouragement.

TABLE OF CONTENTS

Page

LIST OF TABLES

LIST OF FIGURES

Figure Page

Figure Page

CHAPTER 1

INTRODUCTION

With the total global solar module production surpassing 200GW_p, and the average module cost edging towards the sub 0.5 \$/W_p mark [1], higher efficiency cells have become pivotally important. With silicon based solar cells leading the market, and the lab efficiency of such cells reaching 25.6% [2], evermore complicated cell architectures have been introduced. Much of these developments have been in the solar cell contacts, which will be the primary focus of this thesis.

The recent development of complex and diverse contacting schemes in solar cells has introduced contacts ranging from MoO_x and amorphous silicon heterojunctions to tunnel-oxide passivated contacts. The well-established diode theory, which is based on a simple p-n junction, has been proven to be inadequate to intuitively describe the physics and characteristics of these complex contacts.

As results, terminology such as "passivated contacts" and "carrier selective contacts" have been introduced to describe different classes of contacts. However, a clear description of the underlying physics and rigorously defined terminology has been lacking in such efforts. As a consequence, improvement to existing contacts and envisioning novel contacts has been somewhat haphazard and has lacked a clear focus. Here, we attempt to define terminology to describe properties of contacts in a precise and intuitive manner, and introduce a few metrics to evaluate properties of a contact simply and intuitively.

A discussion of an alternative to the traditional diode model has been presented by Würfel et al. [3] which describes the basic operation of solar cells based on first principles in an attempt expel many inaccuracies that have been circulated throughout the scientific

community all too often. As emphasized by Würfel et al., much of the misunderstanding has been a result of viewing all solar cells though the lens of the ideal diode model.

This thesis starts off by revisiting the assumptions and derivation of the diode model, which is discussed in CHAPTER 2. The issues arising from the non-ideal nature of solar cell contacts, as applied to the diode theory is also be briefly discussed here.

The importance of asymmetric conductivity—specifically the roles of asymmetric carrier density and mobility—as elaborated in Würfel et al. is introduced as an alternative theory to the diode model in CHAPTER 3. The theory is introduced from first principles based on the current/transport equations. Furthermore, this approach of describing contact using electron and hole carrier resistances is applied to discuss the properties of contacts in qualitative manner. This discussion will also include a qualitative analysis of a few existing contacts.

CHAPTER 4 will discuss the PC-1D simulation setup that was carried out to test the proposed theory, the results of which are presented in CHAPTER 5. Quantitative metrics that describe the key properties of contacts are presented in this chapter. Furthermore, a combined metric to characterize the contact properties as they affect the efficiency is also given.

A summary of the work presented in this thesis as well as the shortcomings of the prosed theory is included in CHAPTER 6. The chapter concludes with a discussion of possible future work and improvements.

CHAPTER 2

DIODE MODEL

A multitude of theoretical models are useful in understanding and describing the physics of solar cells. For instance, Shockley and Queisser, in their seminal paper [4], used a steam engine model to describe the energy conversion properties of a solar cell. Using thermodynamic detailed balance considerations, they were able to ascertain the ideal band gap of a solar cell that can optimally convert the solar irradiation into electrical power. Using the same methodology, they also established the theoretical upper bound for the efficiency of a silicon solar cell to be 33.3%; a more detailed consideration using a similar model later established that limit to be 29.8% [5].

Although, employing different models to describe a solar cell can provide pivotal insights in to the physics, the one diode model of a solar cell remains the most ubiquitously used one in the field of photovoltaics. Such a propensity is probably because the diode is one of the most fundamental and well-understood devices in the field of electrical engineering. Traditional solar cells, which essentially contain a p-n junction, have many commonalities with diodes; therefore, there is a natural allure to describing solar cell operation using the traditional terminology used to describing diodes. However, some key aspects that are vital to a deeper understanding of solar cells get confounded in such a description. Most of this chapter will attempt to illuminate the one diode model of a solar cell with some discussion on alternate circuit models.

The obvious and main difference between a diode and a solar cell is optically generated current and/or voltage in the latter. At a relatively early stage in solar cell development, it was proposed that superposition of currents and voltages can be applied to

solar cells [6]. This allows the decoupling of the optically driven, power generation process from the diode-like, power dissipation processes inside the solar cell. The circuit model illustrated in Figure 1 is a result of applying the superposition principle to a solar cell. The current source shown, I_L, denotes the current due to the optical generation inside the solar cell. The diode denotes the losses due to recombination, while the series resistance, R_{series}, and the shunt resistance, R_{shunt}, denotes resistive losses.

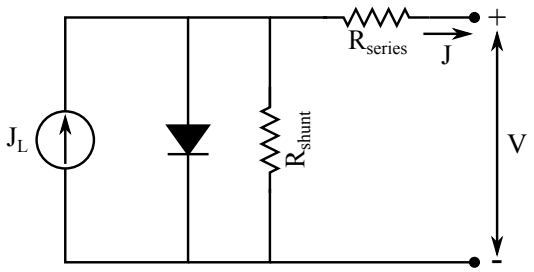

Figure 1 One diode model of a solar cell.

The ideal solar cell current-voltage relationship without any resistive losses is denoted in the following equation.

$$J = J_L - J_0\left(e^{qV/kT} - 1\right) \tag{2.1}$$

When the resistive losses are added as shown in the Figure 1, the equation changes as shown in (2.2).

$$J = J_L - J_0\left(e^{q(V+JR_{series})/kT} - 1\right) - \left(\frac{V + JR_{series}}{R_{shunt}}\right) \quad (2.2)$$

Light generated current (J_L)

Light generated current, is the only variable in the one-diode model that relates to the optical properties of the solar cell. Optical properties of solar cells are a topic that is not extensively covered in this thesis—only a cursory discussion is provide in this section. For deeper discussions about on the topic readers can refer to excellent sources like pveducation.org [7], The Physics of Solar Cells by Jenny Nelson [8], Solar Cell Device Physics by Stephen Fonash [9], or other text books on solar cells.

J_L primarily depends on the materials ability to absorb a photon and create and electron-hole pair. In order to create these charge carriers, the photon must have an energy that is equal to, or larger than, the band-gap of the material. The material's ability to absorb photons and create electron-hole pairs are denoted by parameters such as absorption coefficient and absorption length. Although parasitic absorption—in which the full energy of the absorbed photos does not contribute to carrier generation—does occur, in general, the higher the absorption coefficient, the higher the number of optically generated carriers in a given volume of material.

These generated electron-hole pairs are meta-stable and recombine at a characteristic rate determined by the minority carrier lifetime. Therefore, if the solar cell is to have a large I_L, its structure should allow for the efficient extraction of carriers before they can recombine. This ability of a solar cell to extract generated carriers is parameterized by the collection probability. Intuitively, the carrier collection probability will depend on

the lifetime of the carriers and the mobility (or diffusion coefficient) of the carriers in materials that make up the solar cell.

The foundation of the one diode model, the superposition principle, assumes that I_L is independent of the diode behavior of the solar cell, but as will be discussed in the next section of this chapter, lifetime and mobility also play key roles in the diode behavior.

Making the ideal diode equation

The current-voltage relationship of an ideal diode is given by equation (2.3), in which, J is the current density, J_0 is the recombination parameter, q is the unit charge, V is voltage across the diode, k is the Boltzmann constant, and T is the absolute temperature.

$$J = J_0 \left(e^{qV/kT} - 1 \right) \tag{2.3}$$

The derivation of the ideal diode equation considers a p-n junction as shown in Figure 2, and in order to obtain a simple, analytical solution the approximations are invoked [10]:

1. The diode is one-dimensional.
2. The n- and the p-doped sides are completely ionized and the junction is abrupt.
3. The depletion region is devoid of any free carriers, and therefore, has positive (on the n-side) and negative (on the p-side) regions with immobile dopant ions.
4. There are is no net charge outside the depletion region. Therefore, along with 2, electric fields are confined to the depletion region.

5. There is no recombination or generation in the depletion region. Recombination in all other regions—quasi-neutral regions and the surfaces—happens by the Shockley-Read-Hall mechanism.
6. Low-level injection prevails throughout the device, at all operating points.

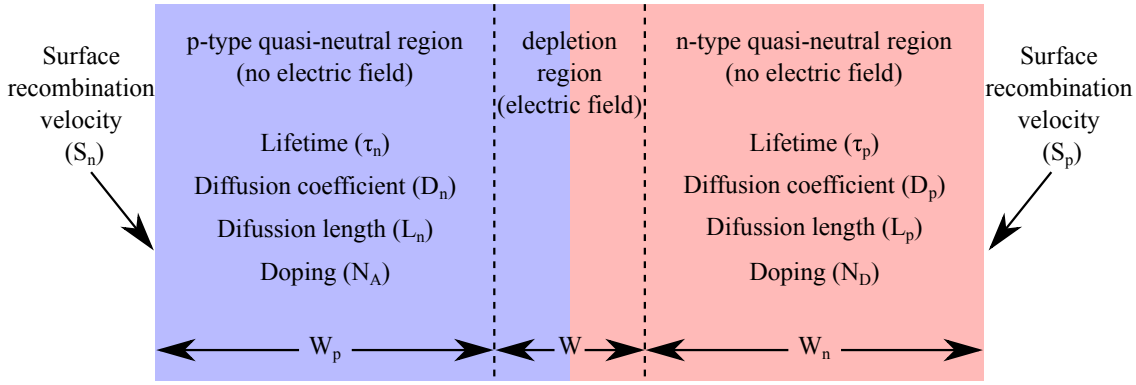

Figure 2 Schematic showing the regions of the ideal p-n junction. The electric fields of each region is shown according to the depletion approximation.

The above equation (2.3) is derived by solving Poisson's equation along with the minority carrier diffusion equation inside the p-n junction (as shown in Figure 2). The former relates the charge distribution with the resultant electric field and the potential distribution; the latter is a combination of the charge transport and continuity equations as applied to a quasi-neutral region. The derivation and an excellent discussion of the minority carrier diffusion equations is given in [11], and the derivation of the diode equation is given in [7], [8], [10].

While the relationships in equation (2.3) and even (2.7) are relatively simple, the device dependent parameters—therefore, all the interesting physics principles—are all

contained in the J_0 , and to a lesser degree in the n, terms. Therefore, a closer look at J_0 term is warranted. The dependence of J_0 on the parameters of the relatively simple, ideal p-n junction illustrated in Figure 2 is given in equation (2.4).

$$J_0 = \frac{qD_n n_i^2}{L_n N_A} \cdot \frac{S_n \cosh(W_p/L_n) + D_n/L_n \sinh(W_p/L_n)}{D_n/L_n \cosh(W_p/L_n) + S_n \sinh(W_p/L_n)} + \frac{qD_p n_i^2}{L_p N_D} \cdot \frac{S_p \cosh(W_n/L_p) + D_p/L_p \sinh(W_n/L_p)}{D_p/L_p \cosh(W_n/L_p) + S_p \sinh(W_n/L_p)} \tag{2.4}$$

While equation (2.4) can be difficult to comprehend at first, it may be simplified for some useful, ideal cases. These are, namely, the wide base diode, and the narrow base diode approximations. The former assumes that all of the recombination occurs in the quasi-neutral region, and the latter, as is the case for conventional Si solar cells, assumes that all of the recombination happens at the surfaces. When these assumptions are invoked, one gets

$$J_0 = qn_i^2 \left(\frac{\mathrm{D}_n}{L_n N_A} + \frac{D_p}{L_p N_D} \right) \tag{2.5}$$

for the wide base diode and

$$J_0 = qn_i^2 \left(\frac{\mathrm{D}_n}{W_p N_A} + \frac{D_p}{W_n N_D} \right) \tag{2.6}$$

for the wide base diode.

Breaking the ideal diode equation

While the assumptions listed above allow for the simple closed form solution, just about all of them get violated when applying the theory to real solar cells. One major violation of the assumptions come in the form of recombination (approximation 5 above). Contrary to the simple assumption, there could be recombination in the depletion region, and more importantly to a solar cell, Auger and band-to-band recombination can dominate the Shockley-Reed-Hall processes in relatively well made cells, in which the defect densities are quite low. These inconsistencies could result in a dramatic difference in the theoretical and actual J-V curves. The general method of addressing this by introducing a a fudge-factor (n), called the ideality factor, modifying equation (2.1) as shown in equation (2.7). The idea is to apply the "right" value for n, at the "right" part of the J-V curve—i.e. the injection level. This however is almost never done in practice for solar cells, and an excellent discussion of this is given by Leilaeioun and Holman in [12].

$$J = J_0 \left(e^{qV/nkT} - 1 \right) \tag{2.7}$$

One common method of addressing this problem is to introduce the two diode model in which one diode represents the ideal Shockey-Reed-Hall recombination, and the other diode represents the non-idealities. The circuit diagram for the two diode model of a solar cell is shown in Figure 3.

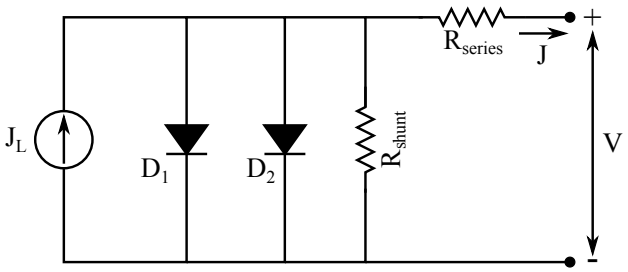

Figure 3 Two-diode model of a solar cell.

The current-voltage equation for the two diode model, as shown in Figure 3 is given in equation (2.8). Here the term starting with J_{01} corresponds to diode, D_1, and the term starting with J_{02} corresponds to diode, D_2. Therefore, the ideality factor of the first diode, n, is assumed to be ≈1, and the ideality factor of the second diode, m, is determined by the other important recombination mechanisms.

$$J = J_L - J_{01}\left(e^{q(V+JR_{series})/nkT} - 1\right) - J_{02}\left(e^{q(V+JR_{series})/mkT} - 1\right) - \left(\frac{V + JR_{series}}{R_{shunt}}\right) \tag{2.8}$$

While the above equation obviously provides a better fit the experimental J-V curves due to the higher number of variables, understanding the physics and the workings of the solar cell becomes more difficult.

Along with the ideality factor, J_0, as shown in equation (2.4) can be difficult to comprehend. The equivalent J_0 equation for a real solar cells with complex structures, which are a far cry from the simple illustration in Figure 2, become extremely convoluted.

For one, none of the modern solar cells have a bulk junction as was assumed for the diode equation derivation. A typical, simple solar cell would have two junctions, a p-n junction and the high-low junctions, and as discussed in the next chapter, these junctions are formed close to the metal interface. Thus, even in a simple case, understanding the recombination, the origin of J_0, and the governing principles of the solar cell with the diode equation can be challenging.

Herein lies the short coming of trying to understand solar cells equipped only with the diode equation. The state-of-the-art solar cells have evolved well beyond the simple approximations of the p-n junction theory. For instance, of the modern high efficiency cells, the passivated emitter and rear cell (PERC) [13] and the passivated emitter, rear locally-diffused (PERL) cell [14] are probably the most closely related designs to the traditional, homo-junction Si solar cell; even those have extremely important 2-D and 3-D effects that cannot be captured or understood easily by a simple J_0 model. Describing and understanding using a simple diode model become even more difficult with Si heterojunction (HIT) solar cells [15]. Even if one assumes the simple Anderson rule of band alignment, a theoretical expression for J_0 becomes mathematically daunting. Moreover, experimentally, the Anderson rule is almost always inadequate, which makes the analysis of heterojunction solar cells using the diode model extremely questionable. Another new class of solar cells that are closely related to the HIT cell is tunnel-oxide passivated contact cell. Fraunhofer ISE [16]–[18] and expanding company in the solar industry Silevo [19], [20] have prosed and produced similar solar cell designs employing tunnel-oxide passivated contacts. The recombination in these cells are also hard to understand by J_0, since the recombination in these cells is limited by transport, and not by

the number of Shockley-Reed-Hall recombination centers, as will be discussed in the next chapter. A good discussion and an attempt to demystify J_0 in solar cells is given by Cuevas in [21].

In summary, the ideal diode equation provides insight and a simple mathematical model to discuss and describe solar cells. The simple assumption made in deriving the ideal diode equations, however, are becoming more and more outdated with the complex solar cell designs that are fabricated today. Therefore, a new approach to thinking about solar cells will help us build an intuitive understanding of these complex structures, and equip us to design better solar cells for the future.

CHAPTER 3

INTRODUCTION II: RESISTANCE MODEL

As discussed in the previous chapter, increasing silicon (Si) solar cell efficiencies depends on reducing recombination—and therefore J_0. It is well understood that in order to achieve the highest efficiencies the total recombination in the solar cell has to be improved until it is only limited by the intrinsic bulk-Si recombination mechanisms [15]. Although practically nontrivial to implement, this can be facilitated by eliminating bulk defects and impurities. Decades of research and development has made it possible to manufacture extremely high quality Si at a feasible cost, and a rich collection of sources discuss methodologies that can achieve these high quality properties [22]. For instance, Czochralski process can now produce Si wafers achieving bulk lifetimes of a few milliseconds.

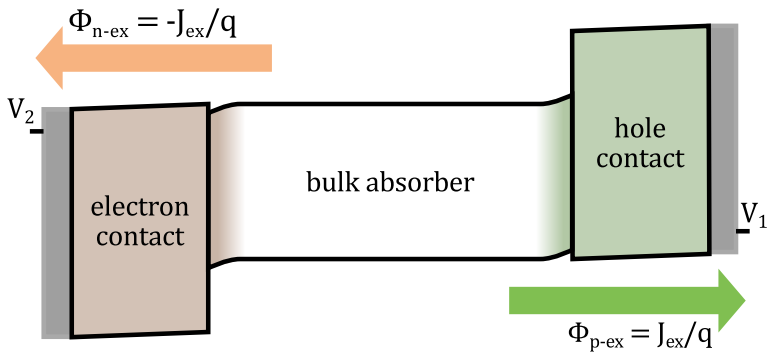

Figure 4 Schematic showing the key regions of a solar cell. A solar cell needs a large absorber region to generate carriers, and two regions on either side to extract electrons and holes separately. At the metallic interface, where the voltage is extracted, should ideally be only one type of carrier.

With these material improvements contributing to low bulk recombination, it is important to have a similar discussion about the recombination in the other regions of the solar cell; in general, the regions that are not part of the bulk region can be thought of as contacts—a deeper discussion of the definition of contacts is included later in this chapter. Therefore, in order to further improve cell efficiencies, improvement of the contact regions is needed. Disparate sources in literature have presented many desirable properties of contacts: carrier selectivity, chemical passivation, field-effect passivation, and low resistance, among others [15]. However, a clear description of the underlying physics and accompanying terminology require unifying concepts previously presented in numerous sources.

Here, we attempt to reinterpret the existing theory required to develop a systematic and comprehensive framework that covers the full spectrum of contacts. This chapter, which is based on the conference proceeding by Koswatta et al. [23], will first discuss the general physics that drive carrier separation in a semiconductor device, followed by a definition of a solar cell contact, based on the generalized design. Next, the two concepts will be combined to qualitatively discuss the desired properties of a solar cell contact. Finally, the terminology and qualitative parameters discussed herein will be applied to discuss a few existing solar cell technologies.

Charge separation

For most modern solar cell designs, with the possible exception of organic solar cells, the contacting regions play a pivotal role in charge separation as well as carrier extraction; the key principles governing carrier transport can be established through the basic equations (3.1) and (3.2) [24], [25]. These equations—*not the minority carrier*

diffusion— are the most basic equations that govern carrier transport. A derivation starting with equations (3.1) and (3.2) and applying the appropriate simplifying approximations to derive the minority carrier diffusion equations is given in [8].

$$J_n = -q\Phi_n = n\mu_n \nabla F_n \tag{3.1}$$

$$J_p = q\Phi_p = p\mu_p \nabla F_p \tag{3.2}$$

In the above equations (3.1) and (3.2), J_n and J_p are electron and hole current densities, n and p are electron and hole densities, μ_n and μ_p are electron and hole mobilities, and ∇F_n and ∇F_p are electron and hole quasi-Fermi-level spatial gradients—the combined terms $n\mu_n$ and $p\mu_p$ are directly proportional to electron and hole conductivities, respectively. Therefore, the key criterion for charge separation in a solar cell—where one type of carrier can flow freely, and the other is blocked—is an asymmetry in conductivity for electrons and holes, *not a built-in electric field.* Therefore, a p-n junction, band-bending, or a built in potential are neither necessary nor sufficient conditions for charge separation in a solar cell. This observation can be intuitively understood by realizing that the conductivities in the above equations are the independent variables that drive quasi-Fermi-level gradients and the current densities. Würfel et al [3] has elaborated the importance of asymmetric conductivity—specifically the roles of asymmetric carrier density and mobility—by means of a few examples. In practice, however, only carrier density can be easily controlled when engineering a solar cell.

In general, carrier concentration is manipulated by varying certain material properties, which include work function, band gap, electron affinity, and density of states.

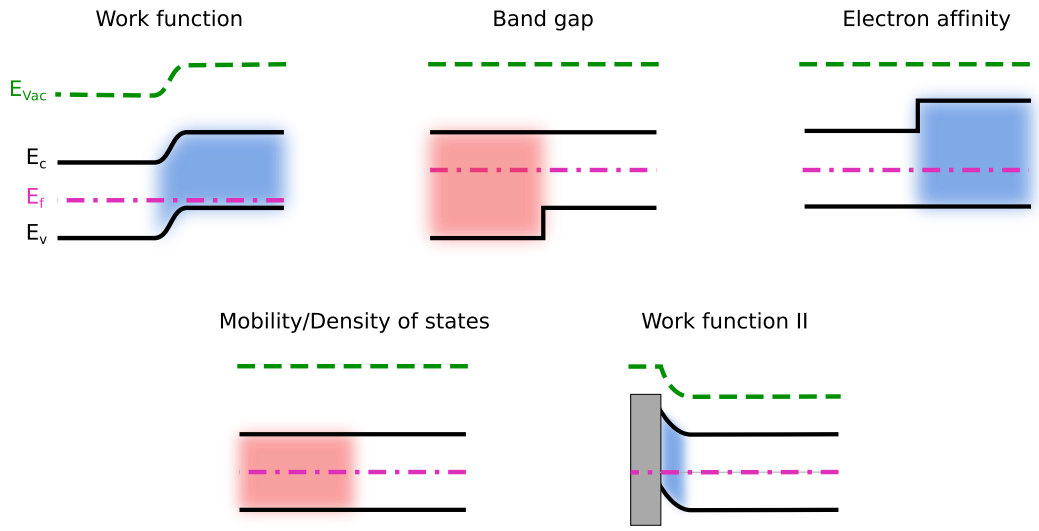

Figure 5 Mechanisms that lead to carrier separation. A change in work function, band gap, electron affinity, and density of states lead to a change carrier concentration. An asymmetry in mobility can also result in carrier separation—the effect is called the Dember potential. A change in mobility or density of states do not appear in the typical energy-vs-distance band diagrams, however, they are practically difficult to manipulate.

A special variation in the first three properties will manifest in the band diagram as a gradient in the conduction band minima and/or valance band maxima; density of states does not readily appear in the typical energy-versus-distance band diagram (Figure 5). Additionally, density of states is difficult to manipulate and is seldom employed in making solar cells. Work function is the most easily manipulated property given that a doping variation, as in the case of a p-n junction, can produce regions of differing electron and hole conductivity in a single semiconductor material. A change in band gap or electron affinity is usually established through a heterostructure. Regardless of how carrier concentration is manipulated, a spatially varying carrier concentration is the only salient factor in practically producing a good solar cell.

The other means of achieving asymmetric carrier conductivities is to change mobility. However, practically achieving this can be difficult. Especially, since the asymmetry of carrier conductivities need to be extremely large ($>10^5$ as will be seen later) for effective charge separation, using mobility as the only means to drive charge separation is impractical. However, most semiconductor materials have a natural asymmetry in mobility of electrons and holes. This factor needs to be taken into consideration, when designing a structure for carrier separation. If not, the asymmetry in carrier conductivity that one hopes to achieve by changing carrier concentration may be undercut—or fortuitously, enhanced—by the asymmetry in mobility. However, since mobility variations do not appear in the typical is energy-vs-distance band-diagram (Figure 5), it is easily overlooked when evaluating a device's ability to separate charge. This probably why the effects of mobility on charge separation is mostly ignored, while the importance of the built-in-potential (in a diode) is often highlighted. However, the effect of asymmetric mobility has been viewed as potential that enhances or or reduces the built-in-potential and has been given the name Dember potential [8].

Definition of a contact

A generalized solar cell structure and the dynamics of light generated carriers in such a device is qualitatively shown in Figure 6. As illustrated, all solar cells consist of a light absorbing material with an optimum band-gap, and two metallic regions at which the voltage and current are extracted (the left and right edges of Figure 6). The typical cell design employs the light absorbing material as the bulk substrate, where most of the

electron-hole pairs are generated, or equivalently[1], where the highest quasi-Fermi-level splitting occurs under illumination. The highly conductive, metal or metal-like regions (for instance, transparent conductive oxides), on the other hand, will only have one Fermi-level under all operating conditions. Therefore, the quasi-Fermi-level splitting must necessarily vanish at the metal/semiconductor interface, and as a corollary, the interface must be highly defective and extremely recombination active.

Employing these key regions common to all solar cells, a contact can be defined as the region starting from the recombination-active metallic interface and spanning the regions designed to be resistive to only one of the carriers—i.e. asymmetrically carrier conductive. To clarify, the metal/semiconductor interface is included as part of the contact, while no part of the bulk regions is included in the contact. As illustrated in Figure 6, although only the regions that are inherently (i.e. *designed* to be) asymmetrically carrier resistive are considered to be a part of the contacts, regions of the the bulk region adjacent to the contact can have induced resistive regions due to the work-function difference between the bulk and the contact. Although these regions are not strictly considered part of the contact, they can play a key roll in the operation of the solar cell, as will be discussed later in this chapter.

[1] $n = n_i e^{(F_n - E_i)/kT}$ and $p = n_i e^{(E_i - F_p)/kT}$, where n and p area electron and hole concentration, respectively. The qausi-Fermi levels F_n and F_p, in-turn, correspond to electrons and holes. The material properties, n_i and E_i values represent intrinsic carrier concentration and intrinsic energy level, respectively.

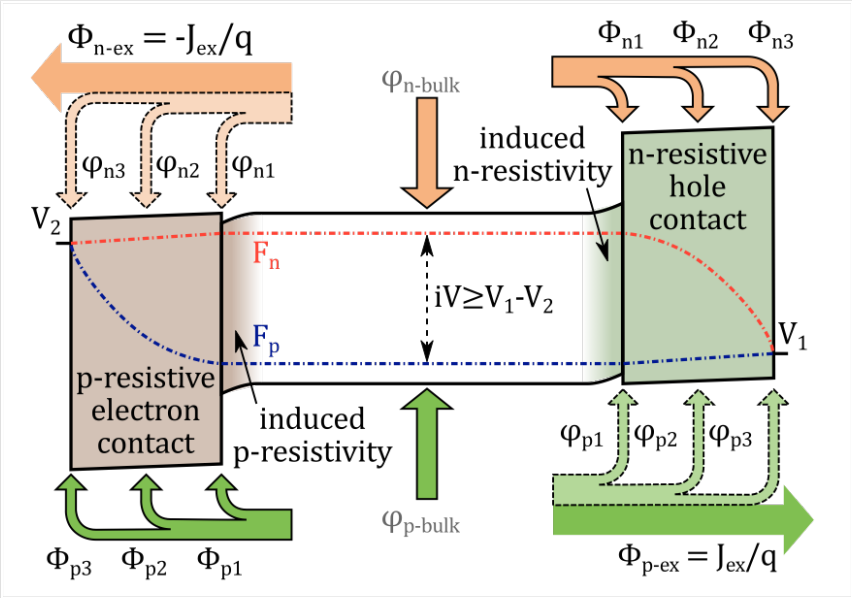

Figure 6 Currents and voltages under illumination for a generalized solar cell with electron- and hole-selective contacts. The magnitudes of the minority-carrier flux of holes (Φ_{p1-3}) and electrons (Φ_{n1-3}) are reflective of the selectivity and passivation qualities of the contacts. The difference between quasi-Fermi-level splitting (iV) and external voltage (V_1-V_2) will additionally depend on low contact resistance for the majority carriers. $\Phi_{n/p\text{-}bulk}$ is commensurate with the bulk quality. Recombination components of the majority carrier fluxes, φ_{n1-3} and φ_{p1-3} will adjust to match Φ_{p1-3} and Φ_{n1-3}, respectively. Bulk Si absorber regions in the vicinity of the contacts can have induced selectivity due a difference in work function between the contact and the bulk.

This proposed definition is only one of many acceptable definitions. For instance, one could define the contact to include the induced resistive regions of the bulk; however, that would suggest that a p-i-n type solar cell only consists of two contacts, which makes this definition too broad. Another option is to define the contacts bases on light absorption—defining the regions that are designed to absorb light as the bulk and the other regions as the contact. However, this definition will exclude any diffused regions, and therefore, the most interesting and important regions of a diffused junction solar cell will

be omitted. Therefore, practically, this definition would only apply to heterojunction contacts rendering it too narrow.

Therefore, defining the contact as the metal interface and the inherently asymmetrically resistive region is a reasonable option; however, this definition is not perfect. For instance, a solar cell with bulk p-n junction (much like the ideal diode schematic in Figure 2), would, according to this definition, consist of only two contacts. However, it is rare to have any modern solar cell design with a bulk p-n junction, and therefore, the author contends that the proposed definition is an adequate one.

Passivation

The primal requirement for a good solar cell is to sustain the largest number of photogenerated carriers, in its bulk without losing them to recombination. For a cell made of high-quality bulk material, in which $\varphi_{0n\text{-}bulk}$ and $\varphi_{0p\text{-}bulk}$ demarcated in Figure 6 are limited by intrinsic Auger and radiative recombination, passivation at the contacts will determine the maximum allowed carrier concentration of the solar cell. While passivation is a term that is used ubiquitously, a closer inspection of the origin of contact passivation is needed. For our discussion, we will employ the minority carrier fluxes of holes ($\Phi_{p1\text{-}3} = \Phi_{p1}+\Phi_{p2}+\Phi_{p3}$) and electrons ($\Phi_{n1\text{-}3} = \Phi_{n1}+\Phi_{n2}+\Phi_{n3}$), as illustrated in Figure 6 to envisage recombination in the contacting regions.

Taking the hole contact in Figure 6 as an example, one can start from the inside of the bulk and work outward to analyze each contribution to the recombination flux. The minority carrier recombination flux components of each region−Φ_{n1}, Φ_{n2}, and Φ_{n3}−will depend on the carrier resistivities of the preceding regions as well as the recombination-

active defect densities of each region. Φ_{n1} is determined by induced electron resistivity and the defect density at the interface between the bulk and the hole contact. Φ_{n1} is thus very closely related to the familiar surface recombination velocity. Similarly, Φ_{n2} is determined by a combination of induced electron resistivity of the bulk and the inherent electron resistivity of the hole contact, and the density of defects inside the hole contact itself. Unlike Φ_{n1} and Φ_{n3}, Φ_{n2} is distributed throughout the hole contact, and therefore, in addition to defect assisted Shockley-Reed-Hall recombination, other recombination can can exasperate Φ_{n2}; especially, Auger recombination can be a pivotal recombination mechanism, since the contacts are typically highly doped. Φ_{n3} is only dependent on the total resistivity (inherent and induced), since the defect density at the outermost interface is necessarily extremely high. The majority carrier recombination fluxes, φ_{p1}, φ_{p2}, and φ_{p3} will match to the minority fluxes, Φ_{n1}, Φ_{n2}, and Φ_{n3}; therefore, the total current out of the solar cell ($J_{ex} = q\Phi_{p\text{-}ex}$) and the amount of recombination are interdependent. Furthermore, it is clear from this analysis that minority carrier resistivity is a key component of contact passivation.

A few key aspects need to be highlighted here. For instance, as mentioned before, there could only be one Fermi-level in the metal. Therefore, at the metal interface, all minority carriers must recombine to collapse the quasi-Fermi-level splitting to zero, under all conditions. Therefore, there could be no reduction of surface defects at the metal/semiconductor interface, and thus, the surface recombination velocity just at that surface would be infinite—in other words, there could be no "chemical passivation" at the metal/semiconductor interface. However, all other interfaces, like those in a

heterojunction could, and should, have chemical passivation—i.e. minimal defect density. Therefore, what is paramount is controlling the flow of carriers to the metal interface, which as discussed, can only be achieved through carrier resistance. Therefore, "field-effect passivation," or more accurately *resistive passivation* that ultimately stops recombination at the metal interface—chemical passivation only matters insofar as minimizing defect densities in the substructure that is put in place to achieve this *resistive passivation,* and thereby, reducing the surface recombination velocity of the contact stack.

Furthermore, as far as achieving passivation, it could be attained via high minority carrier or majority carrier resistance, or both. In other words, although $\Phi_{n1\text{-}3}$ is typically thought of as the limiting flow that drives $\varphi_{p1\text{-}3}$, it could be the other way around. This is why a well design electron contact, a hole contact, or an insulating layer could provide high level of passivation.

Carrier selectivity

Carrier selectivity is a term that is also commonly used to describe a contact. Although, there does not seem to be a formal definition, it is generally used to describe a contact's ability to allow for the one type of carrier while blocking the other. Based on the discussion of the carrier transport, it would seem that this arises due to an asymmetric resistance to one carrier over the other. This is, of course, is intuitively important to a contact, and therefore, the ratio between the electron resistance and hole resistance of a contact could be thought of as a key parameter. A deeper discussion of this aspect will be had in CHAPTER 4, where a quantitative discussion of the nature and importance of carrier selectivity will be introduced.

Majority carrier conductance

Majority carrier conductance or what is usually referred to as "low contact resistance" is, another key aspect of a solar cell contact. However, a few clarifications need to be made in this discussion. For one, many misuse the term "contact resistance" to refer to the series resistance in the full contact. Unfortunately, due to historical reasons, the term "contact resistance" refers only to the barrier to the transfer of charges at the metal/semiconductor interface [26]. Therefore, this "contact resistance" is only one part of the majority carrier resistance in the full contact in a solar cell. Therefore, to eliminate any confusion, majority carrier conductance could be used to refer to the contact's ability to transfer majority carries effectively.

This effect is illustrated as a drop in the majority carrier Fermi-level and an equivalent sloping of the valance and conduction bands in the contacts of Figure 6. Unlike, passivation and carrier selectivity, which could greatly affect the solar cell's open circuit characteristics, majority carrier conductance plays a pivotal roll when there is external current flow in the solar cell, particularly at the maximum power point. Therefore, the efficiency can depend heavily on this parameter.

Application to existing contacts

Figure 7 shows some of the more interesting and commonly used contact technologies. By applying the terminology, we have defined in the previous sections, we can evaluate the strengths and weaknesses of each contact type. Following this evaluation, we believe that the reader will be able to qualitatively evaluate existing contacts and judge the merits of other novel contacts.

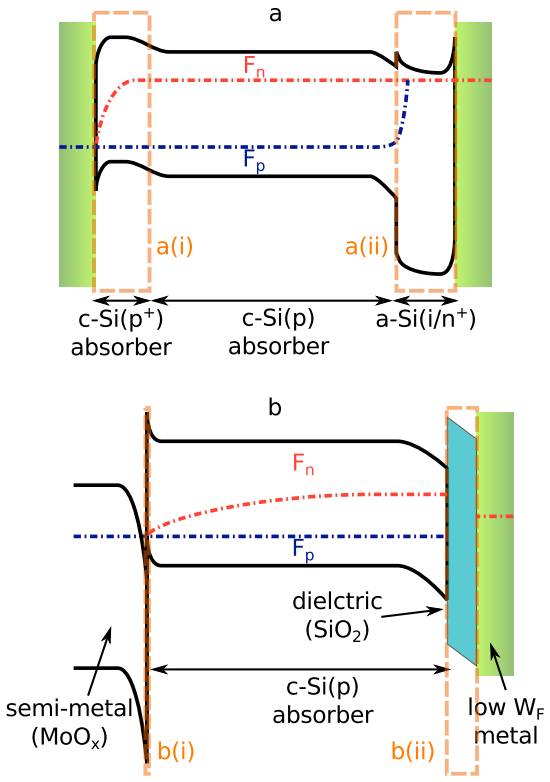

Figure 7 Band diagrams at maximum power point of a *p*-type c-Si device with, (a), a p^+ area as a hole-selective contact on the left and an *i/n* a-Si heterostructure as an electron-selective contact on the right, and (b) a semi-metallic contact on the left and a tunnel-oxide Schottky contact as electron-selective contact on the right.

The contact in Figure 7 a(i) is a Si p^+-p diffused junction with a metal defining its outer edge. The p^+ region has inherent asymmetric carrier resistance due to high hole concentration introduced through doping. Induced asymmetric carrier resistance is formed in the bulk region due to the work function difference between the p and p^+ layers. While these contacts are relatively simple to fabricate, the asymmetry of the carrier concentration

is limited by the doping of silicon and can be further comprised by carrier generation if the contact is under illumination.

The heterocontact Figure 7 in a(ii) is the contact with the most desirable qualities. The combination of large band gap and heavy doping in the a-Si(n^+) layer provides high conductivity for electrons while keeping the hole conductivity low, even under illumination. Induced carrier resistivity—in both the bulk absorber region and the a-Si(i) region—is very important in this device, given that some defects exists in the interface as well as the bulk of the a-Si(n^+) region. A drawback of this contact is that, because of the electron affinity difference of the two materials (seen as a conduction band offset), the conductivity for the majority electrons is lower in the a-Si near the interface than is desired. Furthermore, the mobility of both electrons and holes in a-Si is significantly lower than in c-Si; while this can, and does, help with the passivation, it can have a detrimental effect on the majority carrier conductance. Additionally, there are many defects in the a-Si which can lead to high Φ_2.

A MoO_x contact is illustrated in Figure 7 b(i). MoO_x has been recently studied as a hole-selective contact [27]. The band alignment of the MoO_x/c-Si contact drawn in accordance to Anderson's rule illustrates that it is very similar to a metal/semiconductor contact, in which MoO_x acts as the metal. The large work-function difference between MoO_x and c-Si induces hole resistance in the bulk. In fact, the only asymmetric carrier resistivity of this contact arises from this induced resistivity. Therefore, a great amount of passivation cannot be expected from this type of contact. However, introducing an intrinsic a-Si layer between the MoO_x/c-Si layers will improve the contact as it did in Figure 7 a(ii) [28].

The metal-insulator-semiconductor tunnel contact (Figure 7 b(ii)) provides excellent passivation since the conductivity of minority carriers is very low through the oxide layer. However, the majority carrier conductivity could also be low. Therefore, the only selectivity in this contacts arises from the induced selectivity due to the difference in work function between the metal and the c-Si(p) absorber.

In summary, an alternative to the diode theory of solar cells was presented in chapter. General criteria for charge separation was discussed, in which p-n junctions are only a subsect. Asymmetric carrier resistance was seen to be common to all the different charge separation mechanism. A generalized solar cell structure was employed to first define a contact, and then to evaluate its key properties using carrier resistance. Applying this theory to existing contact structures, it could be seen that an intuitive, qualitative evaluation of various contacting schemes could be easily carried out using the proposed theory compared to the traditional diode theory.

CHAPTER 4

PC1D AND SIMULATION SETUP

In order to understand the resistance based description of contact operation, simulations were carried out using PC-1D [29], [30]. The aim of which was to consider simplified, hypothetical cases that help us understand the important concepts highlighted in CHAPTER 4. Although the assumed simplifications produce idealized results, the understanding that is obtained through these results are general and could be applied to quickly analyze the merits of realistic solar cells.

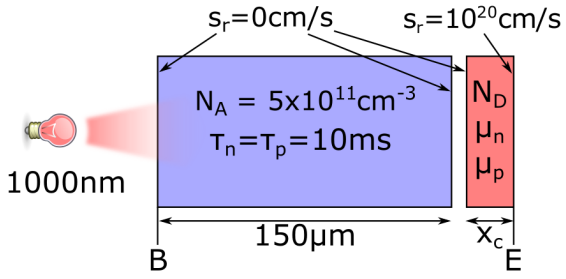

Figure 8 The basic cell structure of the simulated cell. The left conctact was set tob e ideal. The thickness, doping, and electron and hole mobility was changed in the right contact.

To that end, a bulk Si substrate with $5\times10^{11}cm^{-3}$ p-type doping concentration, 150µm thickness, and an assumed electron and hole lifetimes of 10ms was used for all the simulations (Figure 8) . The front infinitesimally thin, hole contact was held constant and assumed to be perfect with no recombination or resistive losses. The back contact was altered by way of changing thickness (x_c), n-type doping concentration (N_D), and electron

(μ_n) and hole (μ_p) mobilities according to Table 1. All the parameters were varied in log space to include a large parameter space, and a total of 10500 simulations were carried out.

Table 1 Variation in material properties of the simulated contacts. Each parameter was changed in log space to cover a larger parameter space. As shown here, a total of 10500 contacts were simulated.

Materials Parameter	Minimum	Maximum	Number of steps (log space)
Electron mobility (μ_e) [$cm^2/V/s$]	10^{-3}	10^4	7
Hole mobility	10^{-1}	10^5	6
Thickness (x_c) [μm]	0.1	10	5
Doping (N_D) [cm^{-3}]	$2x10^{10}$	$2x10^{19}$	50

The result of changing material properties according to above table was to change the electron and hole resistances of the contact over many orders of magnitude. Furthermore, any carrier generation in the contact was turned off by setting the optical absorption to zero—all recombination processes were set to zero except at the metal/semiconductor interface, at which the electron and hole surface recombination velocities were set to 10^{20} cm^2s^{-1}, effectively making the interface infinitely recombination active. All other properties of the back contact were assumed to be the same as those of bulk Si. Furthermore, the structure was illuminated on the front side with a 1000nm monochromatic light source that ensures roughly constant generation throughout the bulk region.

Once the basic PC1D structure as described as shown in Figure 8, the simulation can be implemented as illustrated in the flow chart in Figure 9. The descriptions of the abbreviations used are described in Table 2. The Matlab scripts included in the Appendices

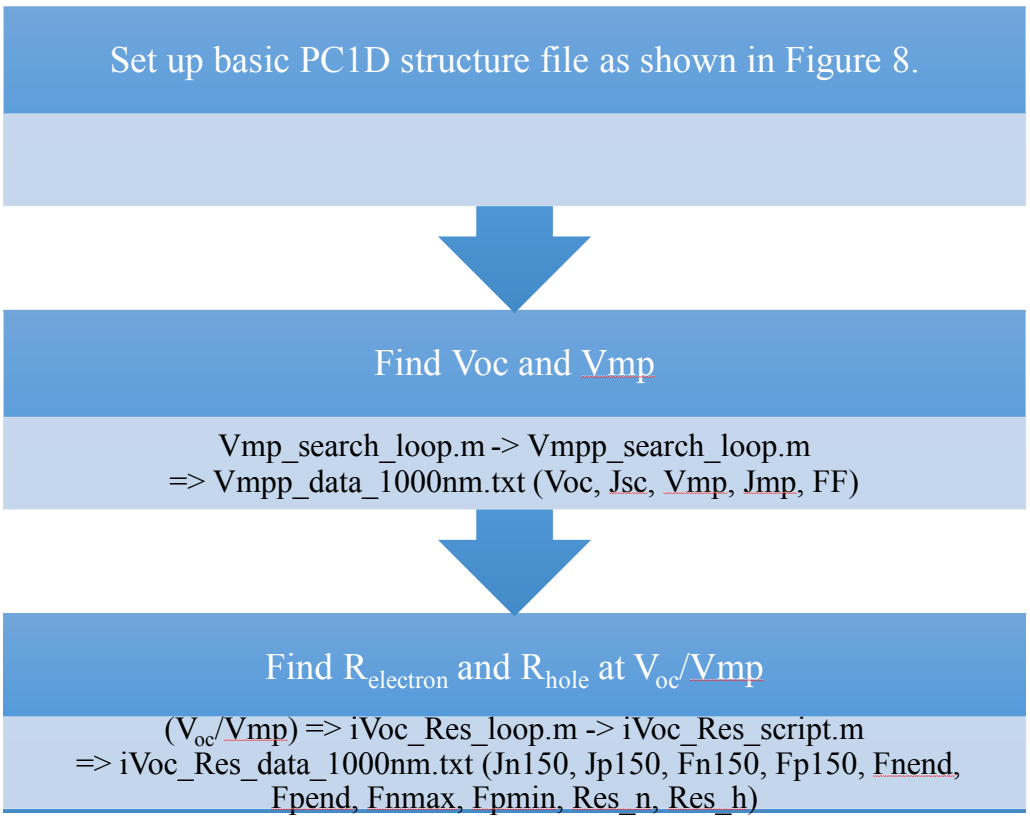

Figure 9 Flowchart of the simulation set up "=>" denotes inputs and outputs to and from Matlab. "->" denotes Matlab scripts calling other Matlab scripts. The terms used in the flow chart is described in Table 2.

A-D utilizes PC1D file "convert_prm_to_ascii.exe" to convert the initial PC1D ".prm" structure file into a editable text file. Then the Matlab scripts can edit the structure file with material parameters defined according to Table 1. Then the Matlab script calls "convert_ascii_to_prm.exe" to convert the text file back to a ".prm" file that could be used in PC1D. Then the new structure file is fed to the "cmd-pc1d5.exe" and Matlab collects the outputs and writes them to a text file. All the .exe files must be in the same folder as the Matlab scripts in order for simulations to run properly. All these files can be are available through the cmd-PC1D version 6.0 download.

Table 2 Abbreviation used in the simulations Figure 9.

Abbreviation	Description
Voc	Open circuit voltage
Vmp	Maximum power point voltage
Jsc	Short circuit current
Jmp	Maximum power point current density
FF	Fill factor
Jn150	Electron current density at the 150μm (beginning of the contact)
Jp150	Hole current density at the 150μm (beginning of the contact
Fn150	Electron quasi-Fermi-level at the 150μm (beginning of the contact)
Fp150	Hole quasi-Fermi-level at the 150μm (beginning of the contact)
Fnend	Electron quasi-Fermi-level at the end of the contact
Fpend	Hole quasi-Fermi-level at the end of the contact
Fnmax	Maximum electron quasi-Fermi-level in the bulk
Fpmin	Minimum hole quasi-Fermi-level in the bulk
Res_e	Specific electron resistivity in the contact
Res_h	Specific hole resistivity in the contact

For each simulation, the electron and hole resistances were calculated according to the following formulas.

$$R_{electron} = \frac{F_{nend} - F_{n150}}{J_{n150}} \tag{4.1}$$

$$R_{hole} = \frac{F_{pend} - F_{p150}}{J_{p150}} \tag{4.2}$$

Each resistance was converted to an electron specific resistivity ($R_{electron}$) and a hole specific resistivity (R_{hole}) with units Ωcm^2, which could be generally applied to a contact with arbitrary surface area.

CHAPTER 5

RESULTS AND DISCUSSION

This chapter presents the data obtained from the PC1D simulations and discusses the results in light of the theoretical framework developed in CHAPTER 3. Namely, the impact of the electron and hole resistance on contact passivation, carrier selectivity and majority carrier conductance will be analyzed using cell performance parameters implied open circuit voltage (iV_{oc}), actual open circuit voltage (V_{oc}), and efficiency, respectively. Furthermore, for each of the contact characteristic discussed, a carrier resistance based metric will be introduced. In order to highlight the physics of the simulated contacts, a few interesting cases will be discussed deeply.

Passivation

As discussed in CHAPTER 3, the internal voltage of a solar cell signifies the carrier concentration, and therefore, the total recombination. The highest internal voltage is achieved at the open-circuit condition and is given the special name, implied open circuit voltage (iV_{oc}). This is equal to the electron and hole quasi-Fermi-level difference in the bulk at open circuit. The quasi-Fermi-level difference, in turn, is related to the total photogenerated electron hole pairs, and as a result, the total recombination, both in the bulk and in the contact, directly affects iV_{oc}. Thus, all else being equal, iV_{oc} can be used as a measure of contact passivation.

The recombination in the contact increases as carriers get generated in the bulk, and since the defect density at the metal interface is, necessarily, extremely high, any electron-hole pair that reaches the interface will quickly recombine. A scheme that mitigates this uncontrolled recombination by curtailing the flow of electrons, holes, or both to the

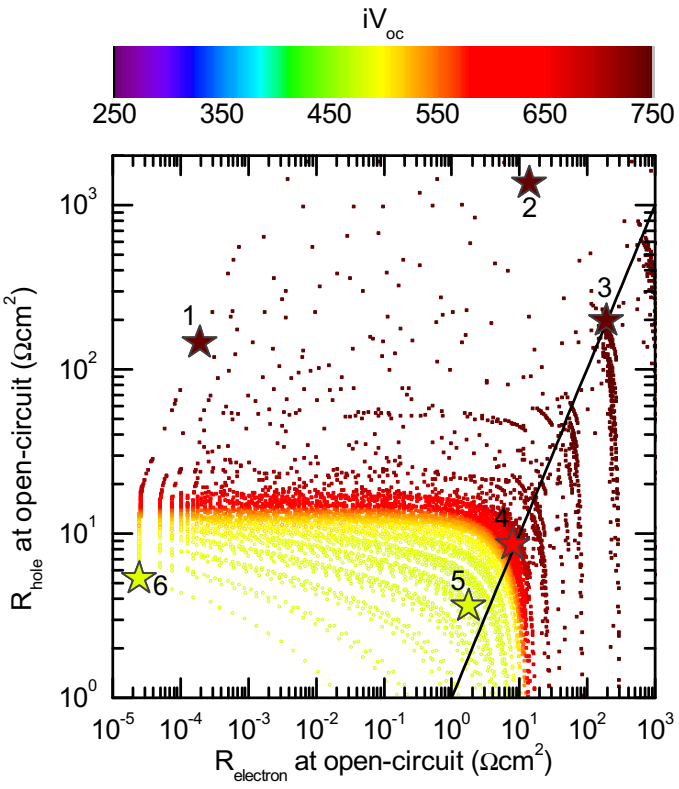

Figure 10 Implied Voc dependence on electron and hole specific resistivity of the contact. $R_{electron}$=R_{hole} line is shown in black.

interface is taken as contact passivation. Therefore, passivation, as predicted by equations (1) and (2), can only be achieved by having high electron resistance ($R_{electron}$), high hole resistance (R_{hole}), or both. The simulated results in Figure 10 show dependence of iV_{oc} on $R_{electron}$ and hole resistance R_{hole} of the contact.

From Figure 10, I could be seen that all the solar cells have an iV_{oc} of at least ~480mV, and good passivation could be achieved for contacts with $R_{electron}$ or R_{hole} larger than ~20 Ωcm^2. As hypothesized, although this contact is supposed to be an electron contact, very good passivation can be achieved with contacts that has a larger $R_{electron}$ than R_{hole}. A line denoting $R_{electron}$ = R_{hole} is shown to easily clarify this observation, and observing contacts 1, 2, and 3, it is clear that large resistances play the biggest role in

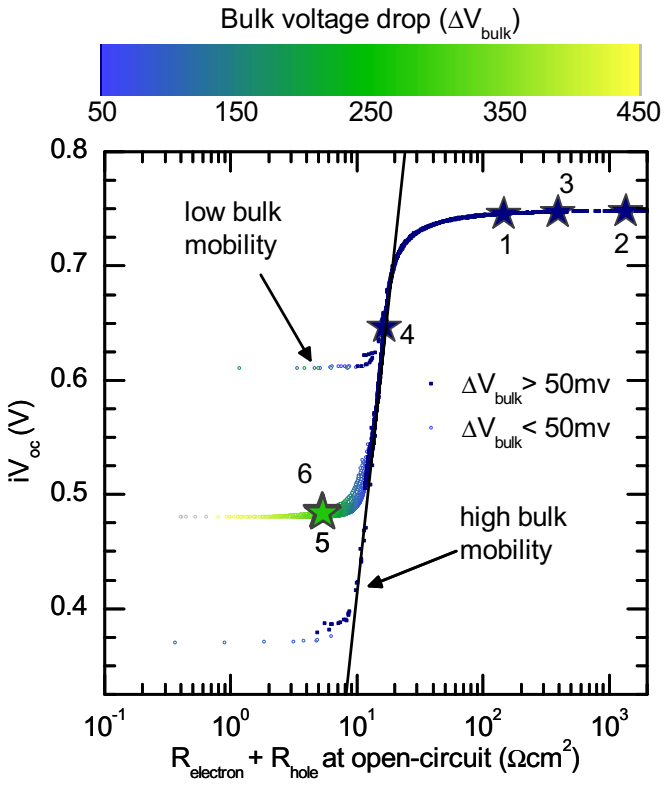

Figure 11 iVoc as a function of the proposed contact passivation metric. Cells with a drop in bulk quasi-Fermi-level (ΔV_{bulk}) larger than 50mV are denoted in a lighter shade.

passivation. Contact 4 provides some passivation, but contacts 5 and 6 provide almost no passivation.

Given the above observation, it is intuitive to quantify the passivation of a contact by using the sum of $R_{electron}$ and R_{hole} as a metric. Figure 11, shows iV_{oc} plotted as a function of $R_{electron} + R_{hole}$. It also shows extra data not show in Figure 10 (a), namely results for cells with artificially high bulk mobility and cells with artificially low bulk mobility. Focusing on just data with normal Si bulk mobilities—i.e. data common to Figure 10 and Figure 11—one can see a clear "S" shape with iV_{oc} saturating at a maximum of around 750mV and a minimum of around 480mV. The iV_{oc} changes rapidly with $R_{electron} + R_{hole}$

for its values between around 0.8 Ωcm^2 to around 50 Ωcm^2. Essentially, the metric $R_{electron}$ + R_{hole} only predicts the iV_{oc} with in this range. This is because at the high end, in which the contact passivation is excellent, the passivation is limited by bulk recombination. Therefore, change in the contact passivation quality is not going to change the iV_{oc} commensurately. The more interesting phenomenon is at the lower end; making the passivation of the contact worse does not seem to make the iV_{oc} much worse. This can be attributed to the resistance of electrons and hole in the bulk—since the electrons and holes created in the bulk has to move to the contact to recombine, there is a resistance associated with that transport. Therefore, for extremely poorly passivating contacts, the bulk provides some "free" passivation. This hypothesis is confirmed by looking at cells with higher and lower bulk mobilities. A bulk with higher mobility provides a lower resistance path for the carriers to reach the contact, and therefore, has a lower limit for the minimum iV_{oc}. The converse is true for a bulk with lower mobility. Note that the upper limit for iV_{oc} in all three cases are the same, because the bulk lifetime is the same for all three cases. In general, for contacts not limited by the bulk effects, the contact passivation and iV_{oc} would be related by the straight line show in Figure 11.

Furthermore, the switch from bulk dominated to contact limited iV_{oc} happens at the lower end at around $R_{electron}$+R_{hole} of 20Ωcm^2. Around this transition, the data in Figure 11 appears to be fuzzy. This is because the contacts with the same resistances can have different *induced* effects on the bulk given the work function difference between the bulk and the contact. For instance, a contact with lower n-doping but higher mobility will induce a smaller electron conductance in the bulk compared to a contact that has higher n-doing

but lower mobility, even though, the two contacts have the same electron and hole resistances.

A good way to exclude this and other bulk effects for contacts with lower iV_{oc}s is to consider the drop in quasi-Fermi-levels in the bulk. Namely, if the quasi-Fermi-levels (ΔV_{bulk}) of electrons and holes are larger than ~50mV, the bulk plays a significant role in providing the passivation. These points are marked in Figure 10 by lighter colored points. A corollary of a large ΔV_{bulk} drop is that the cells are necessarily bad when iV_{oc}<500mV. Therefore, excluding these cells (including cells 5 and 6) from the next analysis steps does not overlook any interesting cases that are worth close consideration.

Selectivity

Once the maximum possible internal voltage, iV_{oc}, of a solar cell is determined, the maximum possible external voltage, i.e. open circuit voltage (V_{oc}), is of interest. However, V_{oc} encompasses two characteristics of a contact: its passivation and its ability to extract the voltage out of the bulk. This ability to extract the iV_{oc} out as a real V_{oc} is the contact's selectivity, and here it will be shown that the selectivity of a contact, in resistance base terms, can be related to the ratio of the two carrier resistivity of the contact, as qualitatively defined in CHAPTER 3.

The V_{oc} dependence on both $R_{electron}$ and R_{hole} is shown in Figure 12, and from that, it is clear that any contact with $R_{electron}$>R_{hole} has an unacceptably low V_{oc}. In fact, these contacts are of the wrong "polarity," which makes them hole contacts, as opposed to electron contacts. This observation further emphasizes that the doping alone does not make an electron or hole contact. To clarify, although the contacts to the right of the $R_{electron}$=R_{hole}

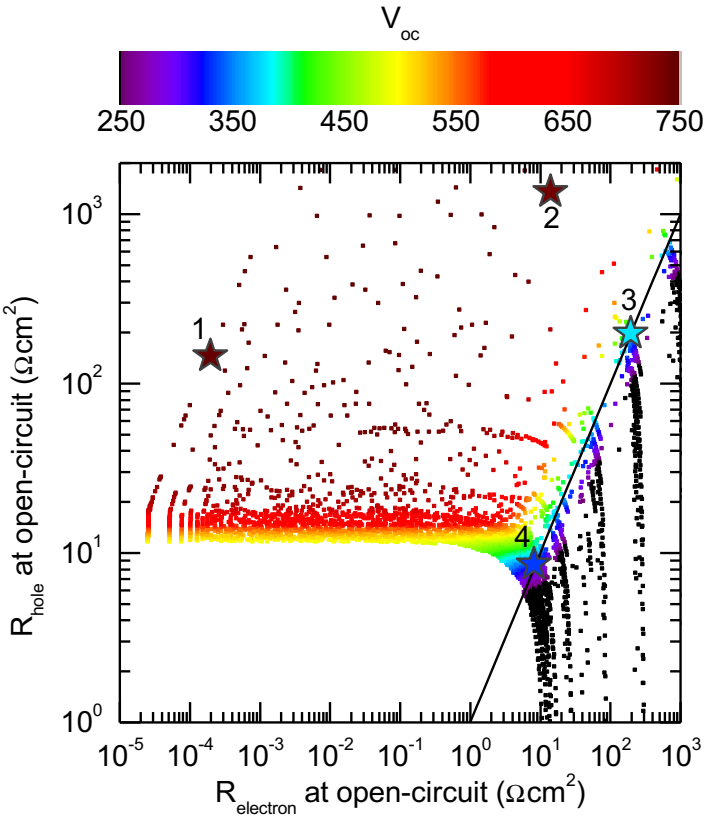

Figure 12 Voc dependence on electron and hole specific resistivities. $R_{electron}$=R_{hole} line is shown in black. Band-diagrams of selected points 1-4 are illustrated in Figure 14.

line have the band bending and the built-in voltage appropriate for an electron contact, they make better hole contacts.

Therefore, unsurprisingly the points that are close to the $R_{electron}$=R_{hole} line, like points 3 and 4 in Figure 11, show diminished Voc compared to iVoc. Points that are further away from the line, like points 1 and 2 have V_{oc}s that are similar to their iV_{oc}s.

Given this trend $R_{hole}/(R_{electron}+R_{hole})$ can be suggested as a metric to measure selectivity. However, since this metric only characterizes selectivity, comparing it directly with V_{oc}, which includes both passivation and selectivity, would be erroneous. Therefore, as shown in Figure 13 (a), it is appropriate to compare the proposed selectivity metric with V_{oc}/iV_{oc},

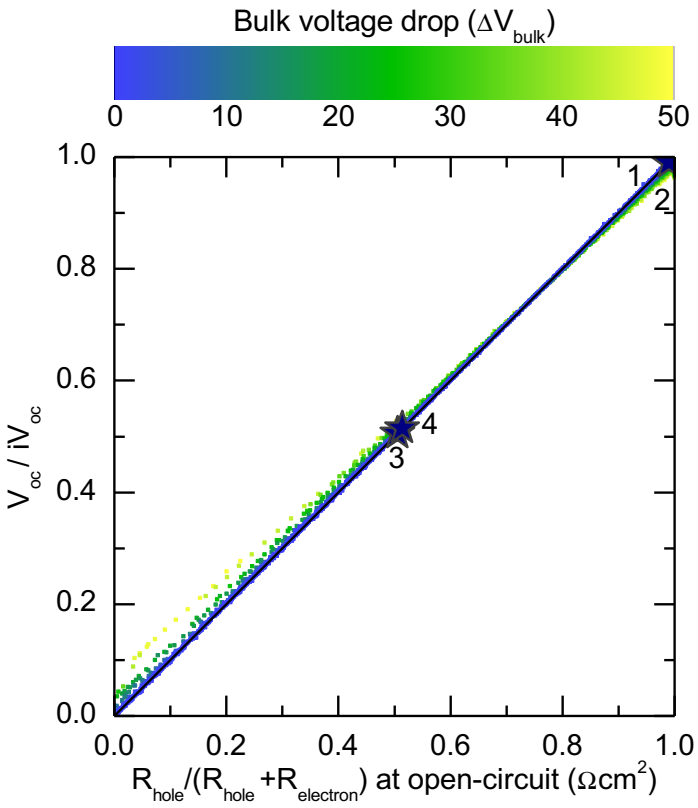

Figure 13 V_{oc}/iV_{oc} dependence on contact selectivity matric $R_{hole}/(R_{hole}+R_{electron})$.

which is essentially V_{oc}, normalized by passivation. Alternatively, a contact under open-circuit conditions can be viewed as a simple voltage splitter in which the iV_{oc} is the supply and V_{oc} is the output.

Figure 13 (a) shows that the proposed metric quantifies selectivity very well. As in the case of the passivation metric, the selectivity metric is also sensitive to the bulk voltage drop (ΔV_{bulk}). In fact, although not shown here, the cells with larger bulk effects (ΔV_{bulk}>50mV) would all fall well outside the y=x line. As expected, Figure 13 (a) demonstrates that points 1 and 2 have good selectivity, essentially converting all the iV_{oc} to V_{oc}. This also shows that the selectivity should be very close to 1 in an acceptable contact.

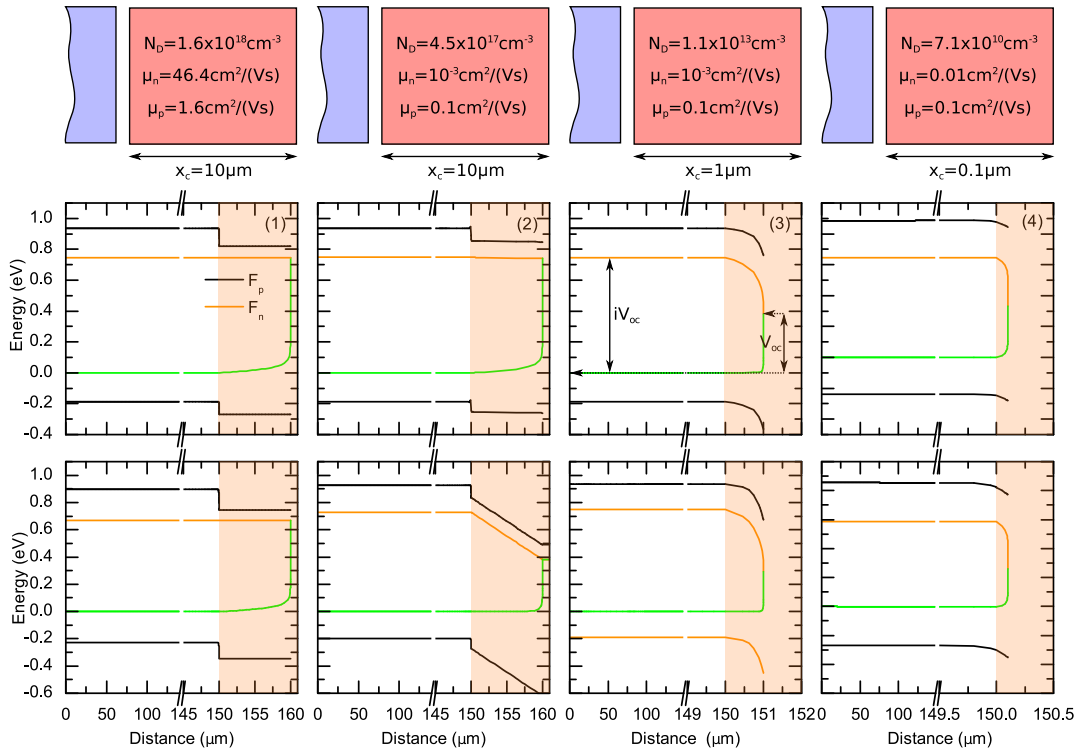

Figure 14 Band diagrams of the selected solar cells under open circuit conditions (top). The same shown in maximum power conditions (bottom). Thicknesses of the contacts are different depending on the cell structure. The band structure is show in greater detail in the vicinity of the contact.

Inspecting the band diagrams of contacts 1-4 shown in Figure 14 (top) clarifies the observations made so far. Contact 4 has lower iV_{oc} due to poor passivation and contact 3 and 4 are unable to convert iV_{oc} effectively to V_{oc}. The poor selectivity is due to the roughly equal drop in electron quasi-Fermi-level (F_n) and hole quasi-Fermi-level (F_p) in the contact.

Majority carrier conductance

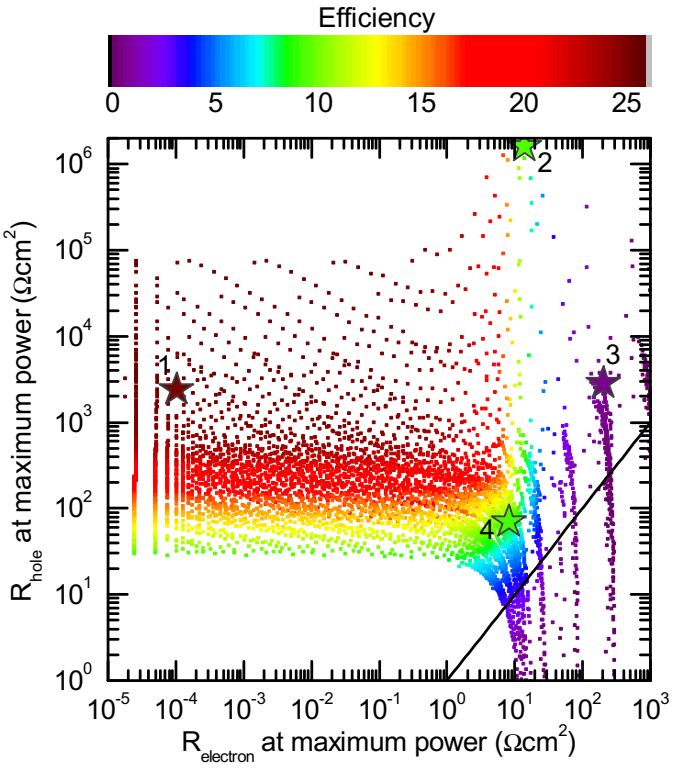

Figure 15 The dependence of efficiency on $R_{electron}$ and R_{hole}. The resistances here are calculated under the open circuit conditions. $R_{electron}$=R_{hole} line is shown for reference.

Since this work has so far pointed out only two variables that characterize a contact, namely, $R_{electron}$ and R_{hole}, defining more than two contact metrics employing the two variables would seem superfluous. However, observing the band diagrams in Figure 14 (bottom) shows that the passivation and selectivity metrics do not fully capture the performance of the solar cell. Namely that the cell 2 has a massive drop in voltage in the contact at the maximum power point condition. This is also observed in the efficiency map shown in Figure 15. Both cell 1 and 2 have high passivation and selectivity, however, contact 2 has a lower majority carrier conductance. Therefore, it must be that a contact

should have high passivation, selectivity, and low majority carrier conductance. Since only two of these metrics could be independent, a contact that has high passivation and low majority carrier conductance would meet all the sufficient conditions for a good contact; such a contact would automatically have high selectivity.

Combined metric

We can combine the metrics discussed above to one metric to describe the characteristics of a contact. The proposed metric is given in equation (5.1). Here the majority carrier resistance is the first term. As discussed above, the majority carrier conductance plays a large role in determining the efficiency of the solar cell. In the second term, focusing on the denominator, $R_{electron}+R_{hole}$ could be recognized as the passivation provided by the contact. The numerator is only a fudge factor so that the passivation and the majority carrier conductance are scaled appropriately.

$$Metric = R_{electron} + \frac{1000}{R_{electron} + R_{hole}} \tag{5.1}$$

The dependence of the efficiency on the proposed metric is shown in Figure 16. While the metric seems to describe the efficiency adequately well, there is some spreading in the data. A better fit may be achieved with further optimizing the fudge factor. Additionally, ΔV_{bulk} does not seems to correspond very well with the performance of the contact—contacts corresponding to both high and low efficiencies have low ΔV_{bulk}. This may be because the bulk effects get compounded in the above metric to a certain degree.

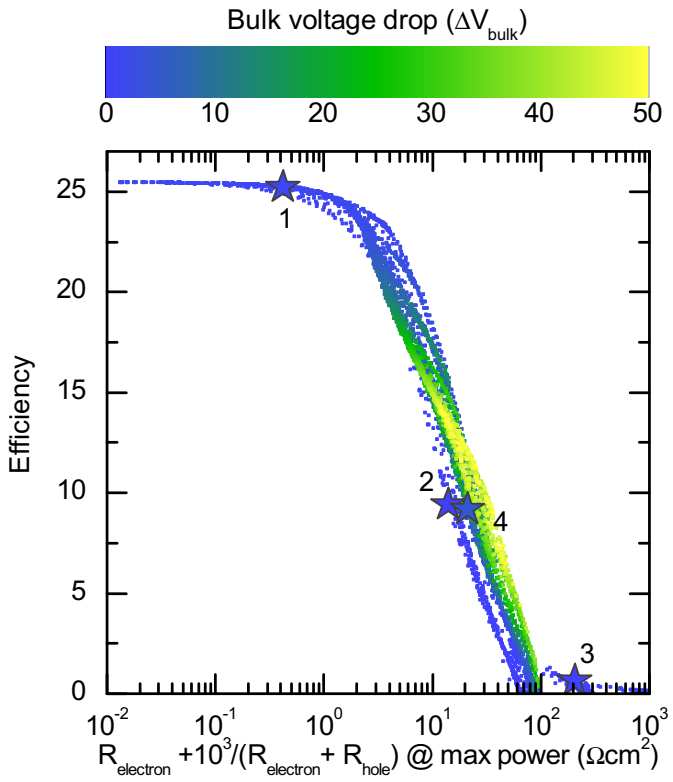

Figure 16 The dependence of efficiency on the proposed combined metric.

However, further study is needed to accurately determine the underlying effects that govern the observed effects.

One salient point to note is that the electron and hole resistance in the contacts need to be calculated for the given operating point of the solar cell. Therefore, each point of a I-V curve would have a unique $R_{electron}$ and R_{hole} values. This was taken into consideration in Figure 10, Figure 11, Figure 12, and Figure 13 ($R_{electron}$ and R_{hole} calculated under open circuit conditions), and Figure 15 and Figure 16 ($R_{electron}$ and R_{hole} calculated under maximum power conditions). While this changing resistances may seem contradictory to the traditional view of a resistor, which is usually thought to have a constant resistance, the

underlying physics used in this approach is incontrovertible. Furthermore, even traditional resistors seldom have truly linear I-V curves with a constant resistance throughout their operating regime. For instance, due to temperature effects, the resistance can change with higher current flow. This, like in the case of $R_{electron}$ and R_{hole} in the solar cell contacts, does not contradict the physics (i.e. Ohm's law) that is applied to the resistor, as long as the appropriate resistance value is used.

CHAPTER 6

CONCLUSION

Simulations were presented to show the validity of the proposed model, and quantitative metrics were proposed to characterize the properties of a contact. It was shown that just carrier selectivity and passivation by themselves were not sufficient conditions for a good contact; rather passivation and majority carrier conductance meet the necessary and sufficient conditions to making a good contact. Finally, a combined metric was proposed to describe the contact's effect on the efficiency.

While this theoretical study was carried out to help the intuitive understanding of contacts, and help imagine better contacts for the future, experimental characterization of the proposed contact metrics remain challenge. Specifically, since there are no readily available methods to measure the minority carrier resistance, novel approaches in characterization maybe necessary to advance the discussion presented in this thesis further. Others that have tried to characterize novel contacts have used a recombination parameter of the contact (J_{0c}) and contact resistance (ρ_c) instead of the minority and majority carrier resistances, respectively [31]. These measurable quantities are shown in the form of a map of efficiencies in Figure 17. This map is comparable to the efficiency map shown in Figure 15. However, further study is needed to show the direct correlation between minority carrier resistance and J_{0c}. It must be noted that ρ_c, that is referred to as the "contact resistance" in [31] is the same as the majority carrier resistance mentioned in this thesis.

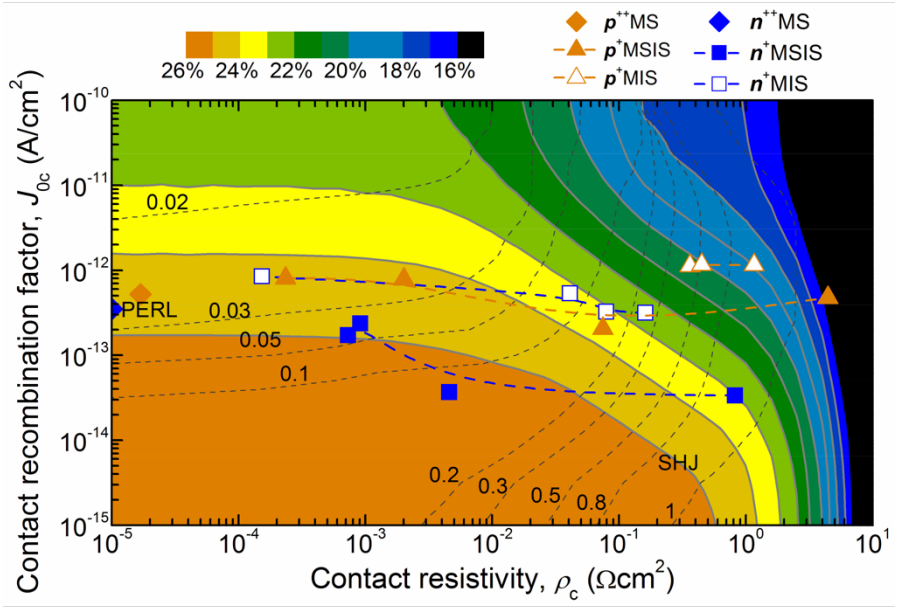

Figure 17 Simulated optimum contact fraction (dotted lines) and resultant efficiency (contour plot) as a function of rear contact ρ_c and J_{0c}. Results presented in [31] are superimposed over the contour plot. From [31].

To further elucidated the measurement techniques used in [31], a method to measure the recombination parameter of the contacting region (J_{0c}) was proposed by Kane et al. [32]. Here, the J_{0c} contribution is decoupled from the overall recombination parameter (J_0) of the solar cell using quasi-steady-state photoconductance measurements. Since, the metal can significantly alter the conductance measurement, this method becomes challenging when the metal coverage is high. Furthermore, the transfer length method (TLM) can be used to measure the ρ_c of a contact [33]. Although this measurement technique was originally designed to measure the resistances between just two interfaces, it has been applied to stacks of layers with some success.

While the experimental implementation of the parameters discussed in this thesis require further study, the theoretical framework and physics outlined here are applicable to

all types of solar cell contacts. An electron- and hole-resistance-based approach to describing the characteristics of contacts was shown as an alternative to the diode model. The proposed model was shown to be more intuitive in describing a plethora of different contacts and their main features, namely passivation, carrier selectivity and majority carrier conductance. While the simulations and the theories explored in this thesis discuss the properties of an electron contact, the insights gained can be applicable to hole contacts without difficulty. Furthermore, the same theories and principles can be extend beyond c-Si solar cells to apply other PV technologies.

REFERENCES

[1] "International Technology Roadmap for Photovoltaic (ITRPV): Results 2015," *ITRPV*, 2016. [Online]. Available: http://www.itrpv.net/.

[2] K. Masuko, M. Shigematsu, T. Hashiguchi, D. Fujishima, M. Kai, N. Yoshimura, T. Yamaguchi, Y. Ichihashi, T. Mishima, N. Matsubara, T. Yamanishi, T. Takahama, M. Taguchi, E. Maruyama, and S. Okamoto, "Achievement of More Than 25% Conversion Efficiency With Crystalline Silicon Heterojunction Solar Cell," in *Photovoltaic Specialists Conference*, 2014, pp. 1–3.

[3] U. Würfel, A. Cuevas, and P. Würfel, "Charge Carrier Separation in Solar Cells," *IEEE J. Photovoltaics*, vol. 5, no. 1, pp. 461 – 469, 2014.

[4] W. Shockley and H. J. Queisser, "Detailed Balance Limit of Efficiency of p-n Junction Solar Cells," *J. Appl. Phys.*, vol. 32, no. 3, p. 510, 1961.

[5] T. Tiedje, E. Yablonovitch, G. D. Cody, and B. G. Brooks, "Limiting efficiency of silicon solar cells," *IEEE Trans. Electron Devices*, vol. 31, no. 5, pp. 711–716, 1984.

[6] F. A. Lindholm, J. G. Fossum, and E. L. Burgess, "Application of the superposition principle to solar-cell analysis," *IEEE Trans. Electron Devices*, vol. 26, no. 3, pp. 165–171, 1979.

[7] C. Honsberg and S. Bowden, "PVEducation," *www.pveducation.org*, 2015. .

[8] J. Nelson, *The physics of solar cells*. London: Imperial College Press, 2003.

[9] S. J. Fonash, *Solar cell device physics*, 2nd ed. Burlington, MA: Academic Press, 2010.

[10] R. F. Pierret, *Semiconductor Device Fundamentals*. Addison-Wesley, 1996.

[11] R. F. Pierret, *Advanced Semiconductor Fundamentals*, 2nd ed. 2002.

[12] M. Leilaeioun and Z. C. Holman, "Accuracy of Expressions for the Fill Factor of a Solar Cell in Terms of its Open-Circuit Voltage," *Submitted*, 2015.

[13] A. W. Blakers, A. Wang, A. M. Milne, J. Zhao, and M. A. Green, "22.8% Efficient Silicon Solar Cell," *Appl. Phys. Lett.*, vol. 55, no. 13, pp. 1363–1365, 1989.

[14] J. Zhao, A. Wang, and M. A. Green, "24% efficient PERL structure silicon solar cells," in *IEEE Photovoltaic Specialists Conference*, 1990, pp. 333–335.

[15] S. De Wolf, A. Descoeudres, Z. C. Holman, and C. Ballif, "High-efficiency Silicon Heterojunction Solar Cells: A Review," *Green*, vol. 2, no. 1, pp. 7–24, Jan. 2012.

[16] S. W. Glunz, F. Feldmann, A. Richter, M. Bivour, C. Reichel, H. Steinkemper, J. Benick, and M. Hermle, "The Irresistible Charm of a Simple Current Flow Pattern – 25 % With a Solar Cell Featuring a Full-Area Back Contact," no. September, pp. 8–13, 2015.

[17] F. Feldmann, M. Bivour, C. Reichel, M. Hermle, and S. W. Glunz, "Passivated rear contacts for high-efficiency n-type Si solar cells providing high interface passivation quality and excellent transport characteristics," *Sol. Energy Mater. Sol. Cells*, vol. 120, no. PART A, pp. 270–274, 2014.

[18] F. Feldmann, M. Simon, M. Bivour, C. Reichel, M. Hermle, and S. W. Glunz, "Efficient carrier-selective p- and n-contacts for Si solar cells," *Sol. Energy Mater. Sol. Cells*, vol. 131, pp. 100–104, 2014.

[19] J. B. Heng, J. Fu, Z. Xu, and Z. Xie, "Back junction solar cell with tunnel oxide," 2012.

[20] J. Fu, Z. Xu, J. B. Heng, and C. Yu, "Tunneling-junction solar cell with copper grid for concentrated photovoltaic application," 2015.

[21] A. Cuevas, "The Recombination Parameter J0," *Energy Procedia*, vol. 55, pp. 53–62, 2014.

[22] A. Jouini, D. Ponthenier, H. Lignier, N. Enjalbert, B. Marie, B. Drevet, E. Pihan, C. Cayron, T. Lafford, and D. Camel, "Improved multicrystalline silicon ingot crystal quality through seed growth for high efficiency solar cells," *Prog. Photovoltaics Res. Appl.*, vol. 20, pp. 735–746, 2012.

[23] P. Koswatta, M. Boccard, and Z. Holman, "Carrier-Selective Contacts in Silicon Solar Cells," in *Photovoltaic Specialists Conference, 2015*, 2015, no. 2, pp. 1–4.

[24] S. M. Sze and K. N. Kwok, *Physics of Semiconductor Devices*, 3rd ed. Hoboken: Wiley, 2006.

[25] P. Würfel, *Physics of Solar Cells: From Basic Principles to Advanced Concepts*, 2nd ed. Weinheim: WILEY-VCH, 2009.

[26] H. H. Berger, "Contact Resistance and Contact Resistivity," *J. Electrochem. Soc.*, vol. 119, no. 4, pp. 508–14, 1972.

[27] J. Bullock, A. Cuevas, T. Allen, and C. Battaglia, "Molybdenum oxide MoOx: A versatile hole contact for silicon solar cells," *Appl. Phys. Lett.*, vol. 105, no. 23, p. 232109, Dec. 2014.

[28] C. Battaglia, S. M. de Nicolas, S. De Wolf, X. Yin, M. Zheng, C. Ballif, and A. Javey, "Silicon heterojunction solar cell with passivated hole selective MoOx contact," *Appl. Phys. Lett.*, vol. 104, p. 113902, 2014.

[29] P. A. Basore, “Numerical Modeling of Textured Silicon Solar Cells Using PC-1D,” *IEEE Trans. Electron Devices*, vol. 37, no. 2, pp. 337–343, 1990.

[30] H. Haug, A. Kimmerle, J. Greulich, A. Wolf, and E. Stensrud Marstein, “Implementation of Fermi-Dirac statistics and advanced models in PC1D for precise simulations of silicon solar cells,” *Sol. Energy Mater. Sol. Cells*, vol. 131, pp. 30–36, 2014.

[31] J. Bullock, D. Yan, A. Cuevas, B. Demaurex, A. Hessler-Wyser, and S. De Wolf, “Passivated contacts to n+ and p+ silicon based on amorphous silicon and thin dielectrics,” *2014 IEEE 40th Photovolt. Spec. Conf.*, pp. 3442–3447, Jun. 2014.

[32] D. E. Kane and R. M. Swanson, “Measurement of the emitter saturation current by a contactless photoconductivity decay method,” *IEEE Photovolt. Spec. Conf.*, pp. 578–583, 1985.

[33] D. L. Meier and D. K. Schroder, “Contact Resistance: Its Measurement and Relative Importance to Power Loss in a Solar Cell,” *IEEE Trans. Electron Devices*, vol. 31, no. 5, pp. 647–653, 1984.

APPENDIX A

MATLAB CODE: VMPP_SEARCH.M

```
tic
clear;
close all;

% parvalues{215} = num2str(emob(i));
% parvalues{229} = num2str(hmob(i));
% parvalues{332} = num2str(Thickness(i));
% parvalues{337} = num2str(BkgndDop(i));

index = [215; 229; 332; 337;];
emob = logspace(-3,4,7);
hmob = logspace(-1,5,6);
Thickness = logspace(-1,1,5)*1e-4;
BkgndDop = logspace(log10(2e10),log10(2e19),50);
k = 0; % Count simulations
ktotal = length(emob)*length(hmob)*length(Thickness)*length(BkgndDop); % tottal
simulations

fid=fopen('Vmpp_data_1000nm.txt','w');
titles = {'emob','hmob','Thickness','BkgndDop','Voc','Jsc','Vmp','Jmp','FF'};
fprintf(fid, '%s\t',titles{:});

h = waitbar(0,'Starting...','Name','Running simulations'); % Set up simulation progress
report
for i=1:length(emob)
   for ii=1:length(hmob)
      for j=1:length(Thickness)
         for jj=1:length(BkgndDop)
            k = k+1;
            waitbar(k/ktotal,h,sprintf('%d of %d',k,ktotal))
            waitbar(k/ktotal)
            [Voc,Jsc,Vmp,Jmp,FF] = ...
               Vmpp_Search_150327_script(emob(i),hmob(ii)...
               ,Thickness(j),BkgndDop(jj));
            if(Vmp>0)
               Voc = 0;
               Jsc = 0;
               Vmp = 0;
               Jmp = 0;
               FF = 0;
            end
            out = [emob(i)  hmob(ii) Thickness(j) BkgndDop(jj) Voc Jsc Vmp Jmp FF];
            fprintf(fid, '\n');
            fprintf(fid, '%f\t ',out);
         end
```

```
        end
    end
end
fclose(fid);
close(h)
toc
```

APPENDIX B

MATLAB CODE: VMPP_SEARCH_SCRIPT.M

```
function
[Voc,Jsc,Vmp,Jmp,FF]=Vmpp_Search_script(emob,hmob,Thickness,BkgndDop)

filename = '150330Vmpp_Search.prm';


% Convert prm file to plain text
%--------------------------------------------------------------------------
dos(['convert_prm_to_ascii ' filename ' temp_Vmpp_Search.txt']);


% Import parameter names and values from text file, save each in a cell
% array of strings, parnames and parvalues. (Look for "=" to separate names
% from values, if no "=" is found, save entire line in parnames and a blank
% string in parvalues. Note that the length of temp_Vmpp_Search.txt and the indices
% corresponding to each parameter depends on the number of regions in the
% prm file.
%--------------------------------------------------------------------------
temp       = importdata('temp_Vmpp_Search.txt');
parnames  = cell(length(temp),1);
parvalues   = cell(length(temp),1);
for i = 1:length(temp)
   tempi          = temp{i};
   parnames{i}   = tempi(1:strfind(tempi,'='));
   if ~isempty(strfind(tempi,'='))
      parnames{i}   = tempi(1:strfind(tempi,'='));
   else
      parnames{i}   = tempi;
   end
   parvalues{i}    = tempi(strfind(tempi,'=')+1:end);
end

% Optional: Define cfg file from script as well:
%--------------------------------------------------------------------------
%    cfgtext = {'BGN YanCuevas2014;' ,...
%               'Intrinsic Recombination KerrCuevas2002;' ,...
%               'Mobility Klaassen1992;' ,...
%               '//End input//'};
%
%       fid = fopen('configfile_example.cfg','wt');
%       for k=1:length(cfgtext)
%          fprintf(fid, '%s\n', cfgtext{k});
%       end
```

```
% emob    = logspace(-2,5,1000);              % Vector of Rs values to loop through
% FF       = ones(steps,1); % Fill factor vector to calculate
% Voc      = zeros(steps,1);
% Jsc      = zeros(steps,1);
% Vmp      = zeros(steps,1);
% Jmp      = zeros(steps,1);

% h = waitbar(0,'Running'); % Set up simulation progress report
% for i = 1:steps

% Set parameters by modyfing the appropriate line in parvalues. (Look
% through temp_Vmpp_Search.txt to find the correct line number). In a single region
% simulation this line refers to the base series resistance
%--------------------------------------------------------------------------
parvalues{215} = num2str(emob);  % Must be formatted as string
parvalues{229} = num2str(hmob);
parvalues{337} = num2str(BkgndDop);
parvalues{332} = num2str(Thickness);
% parvalues{index} = num2str(new_pram(i));


% Write back to temp_Vmpp_Search.txt:
%--------------------------------------------------------------------------
C   = strcat(parnames,parvalues);
fid = fopen('temp_Vmpp_Search.txt','wt');
for j=1:length(C)
   fprintf(fid, '%s\n', C{j});
end
fclose(fid);

% Convert back to prm file. Use temp_Vmpp_Search.prm if you don't want to make
% changes in the original prm file
%--------------------------------------------------------------------------
dos('convert_ascii_to_prm temp_Vmpp_Search.txt temp_Vmpp_Search.prm');

% Do the simulations with cmd-pc1d.exe or cmd-pc1d6-1.exe. The chosen
% output can be defined by selecting "Graph" -> "Defined" in the GUI.
%--------------------------------------------------------------------------
%     [~,b] = dos('cmd-pc1d6-1.exe temp_Vmpp_Search.prm');
[~,b] = dos('cmd-pc1d5.exe temp_Vmpp_Search.prm');

% Read out the result data
%--------------------------------------------------------------------------
b = strrep(b,'1.#QNAN','NaN'); % Clean up potentially bad data
b = strrep(b,'1.#IND','NaN');
```

```
b = strrep(b,'1.#INF','NaN');
numdata = textscan(b,'%f%f%f%f%f%f%f%f%f%f%f','Headerlines',1);
numdata = [numdata{:}];
data1 = numdata(1,:);
empt2 = not(isfinite(data1));
numdata(:,empt2) = [];

% Read out headers if necessary
%--------------------------------------------------------------------------
%coloumns = length(numdata(1,:));
%firstline = textscan(b,'%s',coloumns,'Delimiter','\t');
%headers = firstline{1};

% Alternative: Use a "silent" mode of PC1Dmod6-1 / PC1D5 instead of
% using cmd-pc1d. (Should give the same results, but sometimes slower
% and with some "flashing")
%--------------------------------------------------------------------------
%       dos('PC1Dmod6-1 /g temp_Vmpp_Search.prm');
%       data = importdata('-pastespecial');
%       numdata = data.data;
%       numdata(end,:) = []; %Sometimes necessary to remove last (bad) data point

% Use output data for calculations
%--------------------------------------------------------------------------
V   = numdata(:,1);
I   = numdata(:,2);
P   = numdata(:,3);

if(length(V)<3 | length(I)<3 )
   Voc  = 0;
   Isc     = 0;
   Jsc   = 0;
   Vmp   = 0;
   Imp     = 0;
   Jmp   = 0;
   FF    = 0;
else
   %    A = str2double(parvalues{212}); % Device area (for a single region simulation)
   A = 10;

   J = 1000.*I./A; % mA/cm2
   Pd = 1000.*P./A; % mW/cm2

   [I1, ind] = unique(I);
   V1    = V(ind);
```

```
    [V2, ind] = unique(V);
    I2      = I(ind);
    Voc   = interp1(I1,V1,0);
    Isc      = abs(interp1(V2,I2,0));
    Jsc   = 1000*Isc/A;
    Vmp   = mean(V(P == min(P)));
    Imp      = abs(mean(I(P == min(P))));
    Jmp   = 1000*Imp/A;
    FF    = abs(100 * Vmp * Imp / ( Voc * Isc ));
end
end
```

APPENDIX C

MATLAB CODE: VIOC_RES_LOOP.M

```
tic
clear;
close all;

%%%%%%%%%%%%%%%% IMPORTANT CHANGE FOR EACH
SIMULATION%%%%%%%%%%%%%%%
num_simulations = 10500;
%%%%%%%%%%%%%%%%%%%%%%%%%%%%%%%%%%%%%%%%%%%%%%%%
%%%%%%%%%%%%%%%%%%%%%%%%%%%%%%%%%

index = [215; 229; 332; 337; 424];
[emob,hmob,Thickness,BkgndDop,Voc,Jsc,Vmp,Jmp,FF] =
importVmpp('Vmpp_data_1000nm.txt', 2, num_simulations+1);
ktotal = length(emob); % tottal simulations

fid=fopen('iVoc_Res_data_1000nm.txt','w');
titles = {'emob','hmob','Thickness','BkgndDop','Voc','Jsc','Vmp','Jmp','FF',...

'Jn150','Jp150','Fn150','Fp150','Fnfront','Fpfront','Fnend','Fpend','Fnmax','Fpmin','Fnmaxp
os','Fpminpos','Res_e','Res_h'};
fprintf(fid, '%s\t',titles{:});

h = waitbar(0,'Starting...','Name','Running simulations'); % Set up simulation progress
report
for k=1:ktotal
    waitbar(k/ktotal,h,sprintf('%d of %d',k,ktotal))
    waitbar(k/ktotal)
    k;
    %% Check if Vmp has unrealistic solutions
    if(Vmp(k)>=0)
        Res_e = -1;
        Res_h = -1;
    else

[Jn150,Jp150,Fn150,Fp150,Fnfront,Fpfront,Fnend,Fpend,Fnmax,Fpmin]=iVoc_Res_150
330_script(emob(k),hmob(k),Thickness(k),BkgndDop(k),Voc(k));
       Res_e = (Fnend-Fn150)/Jn150;
       Res_h = (Fpend-Fp150)/Jp150;
    end
    out = [emob(k)  hmob(k) Thickness(k) BkgndDop(k) Voc(k) Jsc(k) Vmp(k) Jmp(k)
FF(k)...
        Jn150 Jp150 Fn150 Fp150 Fnfront Fpfront Fnend Fpend Fnmax(1) Fpmin(1)
Fnmax(2) Fpmin(2) Res_e Res_h];
    fprintf(fid, '\n');
    fprintf(fid, '%f\t ',out);
```

```
end
fclose(fid)
close(h)

toc
```

APPENDIX D

MATLAB CODE: VIOC_RES_SCRIPT.M

```
function
[Jn150,Jp150,Fn150,Fp150,Fnfront,Fpfront,Fnend,Fpend,Fnmax,Fpmin]=iVoc_Res_scri
pt(emob,hmob,Thickness,BkgndDop,vfinal)

filename = '150330iVoc_Res.prm';


% Convert prm file to plain text
%--------------------------------------------------------------------------
dos(['convert_prm_to_ascii ' filename ' temp_iVoc_Res.txt']);


% Import parameter names and values from text file, save each in a cell
% array of strings, parnames and parvalues. (Look for "=" to separate names
% from values, if no "=" is found, save entire line in parnames and a blank
% string in parvalues. Note that the length of temp.txt and the indices
% corresponding to each parameter depends on the number of regions in the
% prm file.
%--------------------------------------------------------------------------
temp       = importdata('temp_iVoc_Res.txt');
parnames  = cell(length(temp),1);
parvalues   = cell(length(temp),1);
for i = 1:length(temp)
   tempi          = temp{i};
   parnames{i}    = tempi(1:strfind(tempi,'='));
   if ~isempty(strfind(tempi,'='))
      parnames{i}    = tempi(1:strfind(tempi,'='));
   else
      parnames{i}    = tempi;
   end
   parvalues{i}     = tempi(strfind(tempi,'=')+1:end);
end

% Optional: Define cfg file from script as well:
%--------------------------------------------------------------------------
%     cfgtext = {'BGN YanCuevas2014;' ,...
%               'Intrinsic Recombination KerrCuevas2002;' ,...
%               'Mobility Klaassen1992;' ,...
%               '//End input//'};
%
%        fid = fopen('configfile_example.cfg','wt');
```

```
%       for k=1:length(cfgtext)
%          fprintf(fid, '%s\n', cfgtext{k});
%       end

% Set parameters by modyfing the appropriate line in parvalues. (Look
% through temp.txt to find the correct line number). In a single region
% simulation this line refers to the base series resistance
%--------------------------------------------------------------------------
parvalues{215} = num2str(emob);  % Must be formatted as string
parvalues{229} = num2str(hmob);
parvalues{337} = num2str(BkgndDop);
parvalues{332} = num2str(Thickness);
parvalues{424} = num2str(vfinal);

% Write back to temp.txt:
%--------------------------------------------------------------------------
C   = strcat(parnames,parvalues);
fid = fopen('temp_iVoc_Res.txt','wt');
for j=1:length(C)
   fprintf(fid, '%s\n', C{j});
end
fclose(fid);

% Convert back to prm file. Use temp.prm if you don't want to make
% changes in the original prm file
%--------------------------------------------------------------------------
dos('convert_ascii_to_prm temp_iVoc_Res.txt temp_iVoc_Res.prm');

% Do the simulations with cmd-pc1d.exe or cmd-pc1d6-1.exe. The chosen
% output can be defined by selecting "Graph" -> "Defined" in the GUI.
%--------------------------------------------------------------------------
%     [~,b] = dos('cmd-pc1d6-1.exe temp.prm');
[~,b] = dos('cmd-pc1d5.exe temp_iVoc_Res.prm');

% Read out the result data
%--------------------------------------------------------------------------
b = strrep(b,'1.#QNAN','NaN'); % Clean up potentially bad data
b = strrep(b,'1.#IND','NaN');
b = strrep(b,'1.#INF','NaN');
numdata = textscan(b,'%f%f%f%f%f%f%f%f%f%f%f','Headerlines',1);
numdata = [numdata{:}];
data1 = numdata(1,:);
empt2 = not(isfinite(data1));
numdata(:,empt2) = [];
```

```
% Read out headers if necessary
%------------------------------------------------------------------------
%coloumns = length(numdata(1,:));
%firstline = textscan(b,'%s',coloumns,'Delimiter','\t');
%headers = firstline{1};

% Alternative: Use a "silent" mode of PC1Dmod6-1 / PC1D5 instead of
% using cmd-pc1d. (Should give the same results, but sometimes slower
% and with some "flashing")
%------------------------------------------------------------------------
%       dos('PC1Dmod6-1 /g temp.prm');
%       data = importdata('-pastespecial');
%       numdata = data.data;
%       numdata(end,:) = []; %Sometimes necessary to remove last (bad) data point

% Use output data for calculations
%------------------------------------------------------------------------
% Check for unconverged solutions
dim = size(numdata);
if (dim(2)<5)
   Jn150 = 0;
   Jp150 = 0;
   Fn150 = 0;
   Fp150 = 0;
   Fnfront = 0;
   Fpfront = 0;
   Fnend = 0;
   Fpend = 0;
   Fnmax(1) = 0;
   Fpmin(1) = 0;
   Fnmax(2) = 0;
   Fpmin(2) = 0;
else
   dis =  numdata(:,1);
   Jn = numdata(:,2);
   Jp = numdata(:,3);
   Fn = numdata(:,4);
   Fp = numdata(:,5);

Jn150 = mean(Jn(dis == 0.15e-3));
   Jp150 = mean(Jp(dis == 0.15e-3));
   Fn150 = mean(Fn(dis == 0.15e-3));
   Fp150 = mean(Fp(dis == 0.15e-3));
   Fnfront = mean(Fn(dis >= 0.5e-5 & dis <= 1e-5));
   Fpfront = mean(Fp(dis >= 0.5e-5 & dis <= 1e-5));
```

```
    Fnend = Fn(end);
    Fpend = Fp(end);
    Fnmax(1) = max(Fn);
    Fpmin(1) = min(Fp);
    Fnmax(2) = mean(dis(Fn==max(Fn)));
    Fpmin(2) = mean(dis(Fp==min(Fp)));
end
end
```